YbtT is a low-specificity type II thioesterase that maintains production of the metallophore yersiniabactin in pathogenic enterobacteria

Received for publication, September 7, 2018, and in revised form, October 23, 2018 Published, Papers in Press, October 24, 2018, DOI 10.1074/jbc.RA118.005752

Shannon I. Ohlemacher[‡§¶1], Yiqian Xu[‡§¶], Daniel L. Kober[¶‖2], Mahnoor Malik[‡§¶3], Jay C. Nix[‡‡], Tom J. Brett[¶‖**4], and Jeffrey P. Henderson[‡§¶5]**

*From the [‡]Center for Women's Infectious Diseases Research, [§]Division of Infectious Diseases, [¶]Department of Internal Medicine, and [‖]Division of Pulmonary and Critical Care Medicine, **Department of Cell Biology and Physiology, Washington University, St. Louis, Missouri 63110 and the [‡‡]Molecular Biology Consortium, Advanced Light Source, Lawrence Berkeley National Laboratory, Berkeley, California 94720*

Edited by Ruma Banerjee

Clinical isolates of *Yersinia*, *Klebsiella*, and *Escherichia coli* frequently secrete the small molecule metallophore yersiniabactin (Ybt), which passivates and scavenges transition metals during human infections. YbtT is encoded within the Ybt biosynthetic operon and is critical for full Ybt production in bacteria. However, its biosynthetic function has been unclear because it is not essential for Ybt production by the *in vitro* reconstituted nonribosomal peptide synthetase/polyketide synthase (NRPS/PKS) pathway. Here, we report the structural and biochemical characterization of YbtT. YbtT structures at 1.4–1.9 Å resolution possess a serine hydrolase catalytic triad and an associated substrate chamber with features similar to those previously reported for low-specificity type II thioesterases (TEIIs). We found that YbtT interacts with the two major Ybt biosynthetic proteins, HMWP1 (high-molecular-weight protein 1) and HMWP2 (high-molecular-weight protein 2), and hydrolyzes a variety of aromatic and acyl groups from their phosphopantetheinylated carrier protein domains. *In vivo* YbtT titration in uropathogenic *E. coli* revealed a distinct optimum for Ybt production consistent with a tradeoff between clearing both stalled inhibitory intermediates and productive Ybt precursors from HMWP1 and HMWP2. These results are consistent with a model in which YbtT maintains cellular Ybt biosynthesis by removing nonproductive, inhibitory thioesters that form aberrantly at multiple sites on HMWP1 and HMWP2.

The *Yersinia* High Pathogenicity Island (HPI)[6] is a virulence-associated, mobile genetic element found in a number of Gram-negative pathogens, including *Yersinia pestis, Klebsiella,* and uropathogenic *Escherichia coli* (UPEC) (1, 2). The HPI encodes a hybrid nonribosomal peptide synthetase/polyketide synthase (NRPS/PKS) pathway that produces yersiniabactin (Ybt), a small molecule metallophore initially recognized for its role in Fe(III) uptake and more recently found to engage in passivation and uptake of copper and nickel (3–7). Related NRPS/PKS pathways in *Pseudomonas aeruginosa* and *Mycobacterium tuberculosis* produce structurally related siderophores that also facilitate virulence, making these pathways possible antivirulence targets (8).

NRPSs and PKSs are large multidomain enzymes found in bacteria and fungi that produce an immense variety of chemically diverse secondary, or specialized, metabolites. Often likened to an assembly line, these pathways produce complex products from simple precursor molecules, such as amino acids, aryl acids, and acyl-CoAs. NRPS/PKSs consist of modules that incorporate one precursor into the elongating molecule by a series of condensation and modification reactions that are catalyzed by individual domains. Pathway intermediates are covalently attached to dedicated carrier protein domains (CPs) through a thioester bond to the domain's phosphopantetheine (ppant) post-translational modification. The finished products are released from the final CP by a terminal type I thioesterase domain (TEI) present in HMWP1 (9, 10).

The authors declare that they have no conflicts of interest with the contents of this article. The content is solely the responsibility of the authors and does not necessarily represent the official views of the National Institutes of Health.

This article contains Figs. S1–S3.

The atomic coordinates and structure factors (codes 6BA8 and 6BA9) have been deposited in the Protein Data Bank (http://wwpdb.org/).

X-ray diffraction images have been deposited in the SBGrid Data Bank with DOIs 10.15785/SBGRID/631 (PDB 6BA8) and 10.15785/SBGRID/632 (PDB 6BA9).

[1] Supported by National Institutes of Health Training Grant 5T32AI007172-35 from NIAID and National Science Foundation Graduate Research Fellowship Program DGE-1143954.

[2] Supported by National Institutes of Health T32GM007067 and American Heart Association Grants 15PRE22110004 and 17PRE32780001.

[3] Supported by the Summer Focus Program, run by the Young Scientist Program at Washington University.

[4] Recipient of National Institutes of Health Grant R01HL119813. To whom correspondence may be addressed: Box 8052, 660 South Euclid St., St. Louis, MO 63110. E-mail: tbrett@wustl.edu.

[5] Recipient of National Institutes of Health Grants R01DK099534 and R01DK111930 from NIDDK. To whom correspondence should be addressed: Box 8051, 660 South Euclid St., St. Louis, MO 63110. E-mail: hendersonj@wustl.edu.

[6] The abbreviations used are: HPI, High Pathogenicity Island; TEI, type I thioesterase; TEII, type II thioesterase; RMSD, root mean square deviation; ACP, acyl carrier protein; Ybt, yersiniabactin; ppant, phosphopantetheine; CP, carrier protein; NRPS, nonribosomal peptide sythetase; PKS, polyketide synthase; ArCP, aryl carrier protein domain; SAM, *S*-adenosylmethionine; PMSF, phenylmethylsulfonyl fluoride; PDB, Protein Data Bank; IPTG, isopropyl β-D-thiogalactopyranoside; *p*-NP, *p*-nitrophenyl; Ni-NTA, nickel-nitrilotriacetic acid; TCEP, tris(2-carboxyethyl)phosphine; ANOVA, analysis of variance.

The Ybt biosynthetic pathway has been reconstituted *in vitro* with four proteins that are encoded in a single operon on the *Yersinia* HPI: YbtE, HMWP2, HMWP1, and YbtU (3). Biosynthesis begins when the adenylation enzyme YbtE loads salicylic acid onto the first CP of a 230-kDa NRPS called HMWP2. HMWP2 then condenses and cyclizes this salicylic acid unit with 2 units of L-cysteine. The resulting intermediate is next transferred to HMWP1, a 350-kDa hybrid NRPS/PKS that adds a malonyl group from malonyl-CoA, another L-cysteine, and three methyl groups from *S*-adenosylmethionine (SAM). Next, the reductase YbtU acts on an HMWP1-bound intermediate before Ybt is finally released by the TEI (11). A fifth enzyme, YbtT, is encoded on the biosynthetic operon but is not required for *in vitro* reconstitution (3). Nevertheless, *ybtT* deletion mutants of *Y. pestis* and UPEC exhibit severe Ybt production defects (12–14). YbtT possesses a conserved Gly–His–Ser–Xaa–Gly thioesterase motif and is homologous to a class of NRPS/PKS-associated enzymes called type II thioesterases. To date, YbtT has not been biochemically characterized.

Type II thioesterases (TEIIs) are a family of NRPS/PKS-associated enzymes to which a variety of functions has been ascribed (15). The most common and well-understood function is to edit NRPSs and PKSs by removing nonelongatable precursors and intermediates from the CP domains. These erroneous molecules on CPs inhibit the assembly line, and regeneration of the free thiol on the ppant by a TEII salvages the NRPS or PKS for further rounds of biosynthesis. TEII-mediated editing is supported by *in vivo* reduced product levels in TEII deletion mutants and by *in vitro* biochemical characterizations in which TEIIs were shown to hydrolyze small molecules from thioester substrates (15–17). Substrate profiling results from these studies are largely consistent with a role in removing nonelongatable "mistakes," although in a few cases *in vitro* and *in vivo* data suggest another function, such as end product release (18, 19), intermediate release (20), or provision of a key intermediate to a downstream biosynthetic protein (21–23).

Here, we report the first structural and biochemical characterization of YbtT. Crystal structures of *E. coli* YbtT reveal the α/β hydrolase fold and catalytic triad typical of TEIIs. Purified YbtT is an active thioesterase that interacts with HMWP1 and HMWP2. Using LC-MS–based approaches, we found that YbtT cleaves both cognate and noncognate Ybt precursors from acyl-CP domains. YbtT substrate specificity is consistent with an editing activity, the most commonly understood TEII function. The presence of a YbtT activity optimum during *in vivo* and *in vitro* Ybt biosynthesis is consistent with a low-specificity model of editing (17) in which futile hydrolysis of productive precursors competes with restorative hydrolysis of inhibitory thioesters. Optimal Ybt production may thus require a favorable balance between these opposing activities.

Results

YbtT and YbtT–S89A crystal structures

To provide a framework for understanding YbtT function, we crystallized WT YbtT and determined the structure at 1.9 Å resolution (Table 1). YbtT adopts an α/β hydrolase fold with core and lid subdomains (Fig. 1*A*). The core comprises a six-stranded parallel β-sheet encompassed by five α-helices, and the lid (residues 125–173) is formed by three α-helices inserted between β4 and β5 of the core. Analysis for structural neighbors using the DALI server (24) revealed that YbtT shares the highest structural homology with TEIIs from other NRPS pathways: RedJ from *Streptomyces coelicolor* (32% sequence identity) (22) and RifR from *Amycolatopsis mediterranei* (28% sequence identity) (25). It also shares homology with a human TEII associated with fatty acid biosynthesis (22% sequence identity) (Figs. 2, *A* and *B*, and 8*A*) (26). The active site is composed of the conserved serine hydrolase catalytic triad of Ser-89, His-225, and Asp-197 (Fig. 1*B*). The catalytic nucleophile, Ser-89, is located adjacent to the lid domain between strand β3 and helix α3 in the conserved thioesterase motif Gly–His–Ser–Xaa–Gly (Gly-87–His-88–Ser-89–Met-90–Gly-91). The backbone amides of Met-90 and Ala-22 form the oxyanion hole, which serves to stabilize the negative charge that accumulates on the transition state during catalysis. A water molecule occupies the oxyanion hole in the crystal structure. In context with its genetic associations in the Ybt biosynthetic operon, this structure suggests that YbtT functions as a TEII and identifies residues that may be essential for enzymatic activity.

A previous study revealed that alanine substitution mutants in the analogous *Y. pestis* YbtT Ser and His active-site residues could not complement iron-restricted growth of a *ybtT* knockout strain (13). To determine whether this defect specifically reflects loss of catalytic residues or derives from more extensive structural distortion, we crystallized and determined the structure of YbtT–S89A to 1.4 Å resolution. The YbtT–S89A mutant adopts an overall structure very similar to WT, with a Cα RMSD of 0.2 Å (Fig. 1*A*). A minor difference was noted in the orientation of the catalytic triad residues, with the His-225

Table 1
Crystallographic statistics for *E. coli* UTI89 YbtT

Variant	WT	S89A
Data collection statistics		
Space group	$P42_12$	$P42_12$
Unit cell (Å)	$a = 82.3$	$a = 82.5$
	$b = 82.3$	$b = 82.5$
	$c = 81.9$	$c = 82.0$
Source	ALS 4.2.2	ALS 4.2.2
Wavelength (Å)	1.0000	1.0000
Resolution (Å)	58.2–1.90 (1.94-)	58.3–1.40 (1.42-)
R_{merge} (%)	15.4 (389)	6.5 (187)
$CC_{1/2}$	0.997 (0.344)	1.000 (0.303)
Completeness (%)	100 (100)	98.9 (88.0)
Redundancy	11.8 (9.9)	11.9 (5.0)
I/σ (I)	11.2 (0.6)	22.5 (0.7)
Refinement statistics		
R_{work} (%)	19.4	16.6
R_{free} (%)	22.5	18.0
Amino acid residues (#)	249	249
Waters (#)	209	298
RMSD bond length (Å)/angles (°)	0.007/0.886	0.008/0.974
Wilson B ($Å^2$)	30.1	16.8
Average B protein ($Å^2$)	31.6	21.2
Average B water ($Å^2$)	39.5	33.6
Ramachandran		
%Favored	98.0	97.6
%Allowed	2.0	2.4
%Outliers	0	0
Rotamer outliers	0	1
Clashscore	2.86	2.08
Molprobity	1.08	1.00
Luzzati error	0.256	0.150
PDB codes	6BA8	6BA9

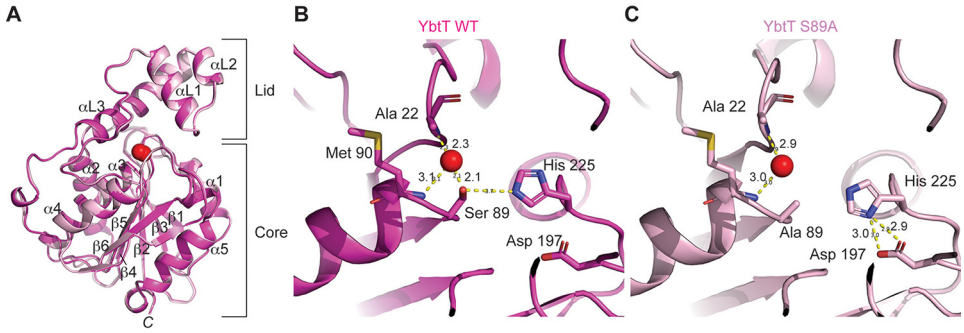

Figure 1. Structure of *E. coli* UTI89 YbtT WT and S89A mutant. *A,* cartoon trace of *E. coli* UTI89 YbtT WT (*magenta*) and S89A (*light pink*) crystal structures. A water molecule found in the oxyanion hole of the active site of each structure is shown (*red sphere*) to mark the location of the active site. Lid and core subdomains are denoted. *B* and *C,* active site of YbtT WT (*B*) and S89A (*C*). Side chains of the catalytic triad (Ser-89, Asp-197, and His-225) and all atoms of the oxyanion hole residues (Ala-22 and Met-90) are shown as *sticks* colored as follows: carbon (*magenta/light pink*); oxygen (*red*); nitrogen (*blue*); sulfur (*yellow*). A water molecule found in each structure in the oxyanion hole is shown as a *red sphere*. Potential hydrogen bonds are shown as *yellow dashes* (distances denoted in Å).

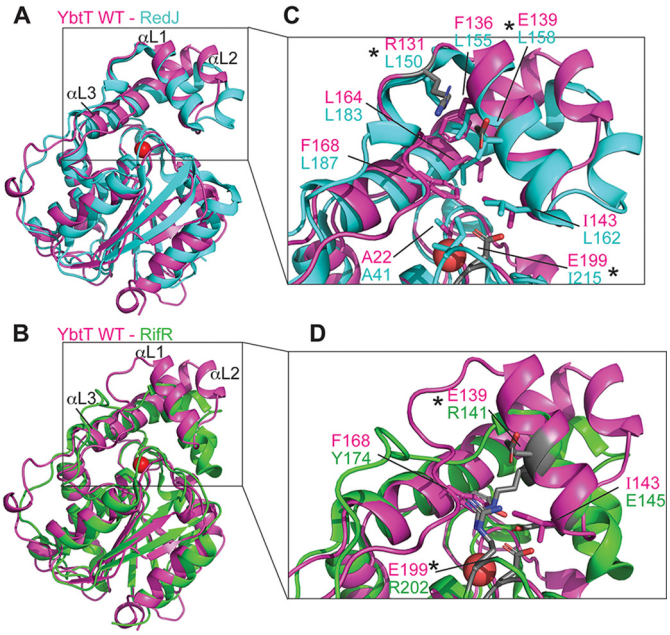

Figure 2. Comparison of YbtT to hybrid NRPS/PKS TEIIs. *A* and *B*, overlay of the crystal structures of YbtT WT (*magenta*) with *S. coelicolor* RedJ (*cyan,* PDB code 3QMV) (*A*) and *A. mediterranei* RifR (*green,* PDB code 3FLB) (*B*). α-Helices that compose the lid subdomain are denoted. The water molecule (*red sphere*) that occupies the oxyanion hole of the active site is shown for reference. *C,* comparison of residues that line the active-site pockets of YbtT and RedJ. Hydrophobic residues lie at these positions in RedJ, and in YbtT some are hydrophobic and others are charged (denoted by *). Hydrophobic residues are colored with carbon atoms *magenta* (YbtT) and *cyan* (RedJ). Carbon atoms of charged residues are colored *dark gray*. Other atoms colored by element are as in Fig. 1. *D,* comparison of polar residues that line the active-site pocket in YbtT and RifR. Polar residues lie at these positions in RifR, and in YbtT some are polar (denoted by *) and some are hydrophobic. Coloring is as in *C*.

imidazole ring in the YbtT–S89A structure flipped relative to its WT orientation (Fig. 1, *B* and *C*). Thus, the S89A mutation did not result in any gross structural changes to YbtT.

Structural comparison of YbtT active site with other NRPS/PKS TEIIs

Previous structural and enzymatic studies of NRPS TEIIs identified active-site features that may contribute to substrate specificity and enzyme function. Differences in substrate specificity between *S. coelicolor* RedJ and *A. mediterranei* RifR have been attributed to residues lining the substrate chamber, which emanate mostly from αL1 and αL3 of the lid domain. In RedJ, these residues are predominantly hydrophobic and at least partially explain its high specificity for substrates with long acyl chains, as opposed to short ones (22). In contrast, several residues lining this pocket in RifR are occupied by polar residues, a feature that likely contributes to the enzyme's low substrate specificity (25). Given these previous observations, we compared residues lining the substrate chamber of YbtT with those of RedJ and RifR for potential functional insights. We found that a number of the positions occupied by hydrophobic residues in RedJ were occupied by charged residues (Arg or Glu) in YbtT (Fig. 2, *A* and *C,* denoted by *). In addition, half of the positions occupied by polar residues in RifR were conserved in YbtT (Fig. 2, *B* and *D,* denoted by *). This analysis suggests that the substrate chamber of YbtT more closely resembles that of RifR, an enzyme that functions as a low-specificity editing TEII, suggesting that YbtT may display similar function and substrate promiscuity.

YbtT flexible lid domain is in an open conformation

Previous structural studies of NRPS TEIIs, both in crystals and in solution, suggest that the lid domain is conformationally flexible and thereby controls substrate access to the active site (22, 25, 27). Indeed, the crystal structures of both RifR and RedJ display multiple lid domain conformations. For RifR, all of the structures display a closed ppant entrance, whereas for RedJ, both open and closed conformations were observed. In YbtT, the αL2 helix is noticeably shifted away from the active site, leaving the lid domain in an open conformation (Fig. 3*A*). Atomic displacement parameter (B-factor) analysis suggests that the YbtT open conformation is likely stabilized by crystal contacts because the B-factors in the lid domain of YbtT are only slightly elevated relative to the core domain. In contrast, the RedJ open conformation displays much higher lid domain B-factors relative to the core (Fig. 3*A*). In the closed conformations of RedJ and RifR, the lid domains also display similar B-factors to the core, likely attributable to several contacts between the lid and core. Comparative cavity and tunnel analysis in CAVER (28, 29) revealed that YbtT has an open ppant entrance that more closely resembles the RedJ open conformation than the blocked ppant entrances of the closed RedJ and

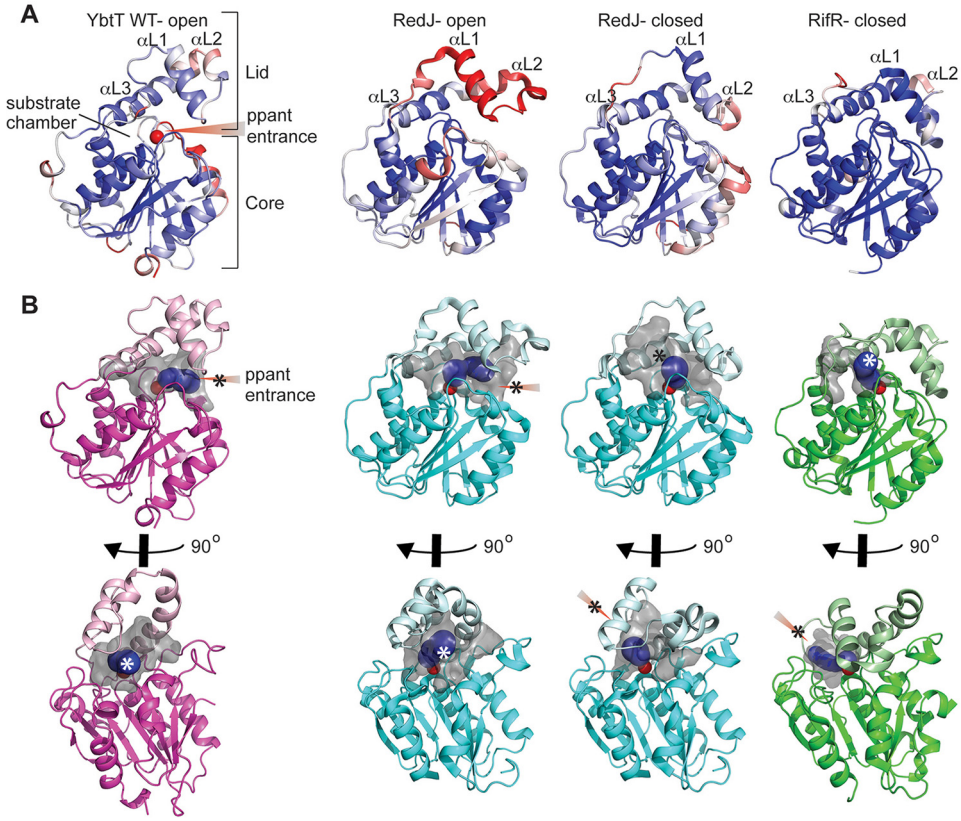

Figure 3. YbtT active site access compared with other hybrid NRPS/PKS TEIIs. *A,* comparison of B-factor distributions and different lid conformations in NRPS/PKS TEII crystal structures. Ribbon structures are colored according to average residue B-factor (*blue* ≤ 20 − *white* − *red* ≥ 50 Å^2). Position of the active site is denoted by the water occupying the oxyanion hole (*red sphere*). The following structures were used for the analysis: *RedJ-open* = 3QMV chain C; *RedJ-closed* = 3QMW chain B; *RifR-closed* = 3FLB. *B,* comparison of ppant entrance tunnels and cavities. Analysis was performed using CAVER (28, 29). Cavities are shown in surface mode and colored *gray*. The most probable tunnels to the active site from the surface detected by CAVER are shown in *dark blue*. Locations where tunnels emerge to surface are denoted by *asterisks* and gradient triangle. Note that YbtT and RedJ are both open at the ppant entrance, whereas RedJ-closed and RifR-closed are not, but they are instead open to a surface displaced about 90° from the putative ppant entrance. Lid subdomains are colored lighter than core subdomains. Cavity volumes calculated by CAVER are: YbtT = 756 Å^3; RedJ-open = 705 Å^3; RedJ-closed = 568 Å^3; RifR-closed = 682 Å^3.

RifR lid subdomain structures (Fig. 3*B*). The open conformations of YbtT and RedJ displayed the largest active site cavities (756 and 705 Å^3, respectively) compared with the closed conformations of RedJ and RifR (568 and 682 Å^3, respectively). Tunnel analysis indicated that the active sites of YbtT and RedJ (open) are accessible from the putative ACP-binding surfaces, whereas RedJ (closed) and RifR are not (Fig. 3*B*). Together, this analysis indicates that our YbtT structure crystallized in an open conformation that displays external access to the active site.

YbtT is an active hydrolase

To determine whether YbtT possesses hydrolase activity, we incubated purified YbtT with the esterase substrates *p*-nitrophenyl (*p*-NP) acetate and *p*-NP butyrate (Fig. 4*A*) under steady-state conditions. *p*-NP esters have been widely used to investigate the *in vitro* activity and substrate specificity of TEIIs (15, 17, 30). Hydrolysis was measured continuously for 10 min, during which time less than 10% of the substrate was converted into product, and the appearance of product was linear as a function of time. YbtT hydrolyzed both esterase substrates, confirming its predicted activity as a hydrolase (Fig. 4*B* and Table 2). The relative velocity of the reaction was proportional to YbtT concentration with both *p*-NP acetate and *p*-NP butyrate (Fig. S1). The poor solubility of *p*-NP butyrate limited the concentrations that could be tested such that only a k_{cat}/K_m value could be estimated. YbtT was inactive with the protease substrate glycine *p*-nitroanilide (Fig. 4, *A* and *C*). The catalytic efficiency of YbtT was low for both *p*-NP substrates (k_{cat}/K_m <50 M^{-1} s^{-1}) compared with other TEIIs tested with the same substrates (15). These esterase substrates are structurally dissimilar from YbtT's hypothesized substrate, an acylated CP, which may contribute to the low measured catalytic efficiencies. These model substrate results demonstrate that YbtT is an active hydrolase.

YbtT serine hydrolase catalytic triad is necessary for activity

To test the hypothesized roles of the serine (Ser-89), histidine (His-225), and aspartic acid (Asp-197) catalytic triad residues in hydrolase activity, we constructed single Ala substitutions at each residue and tested them for hydrolase activity with *p*-NP acetate. YbtT–H225A and YbtT–D197A displayed elution profiles on a gel-filtration column identical to WT and YbtT–S89A, suggesting that these mutations did not grossly alter protein structure (Fig. S2). All three catalytic triad mutants were unable to hydrolyze *p*-NP acetate (Fig. 4*C*). Phenylmethylsulfonyl fluoride (PMSF), a general covalent inhibitor of serine hydrolases, inhibits YbtT activity, as has been shown for other

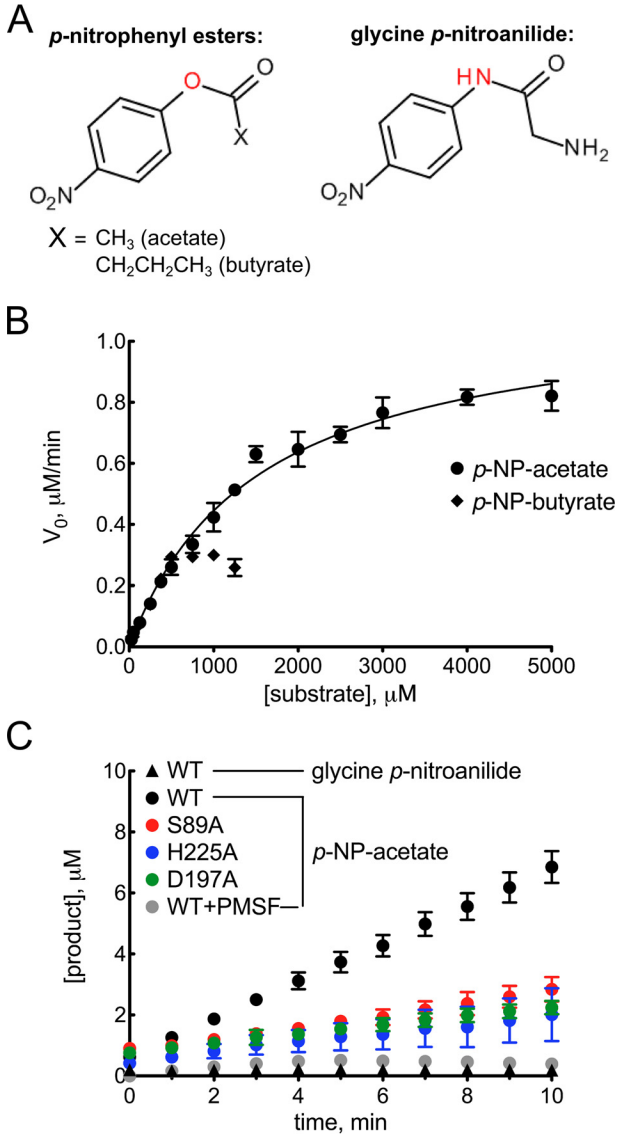

Figure 4. YbtT hydrolyzes ester substrates with short acyl chains, and this activity depends on Ser-89, Asp-197, and His-225. *A,* chemical structures of the substrates used in the activity assays. The ester and amide groups in the *p*-NP esters and glycine *p*-nitroanilide, respectively, are marked in *red*. *B,* Michaelis-Menten plot for hydrolysis of *p*-NP acetate and butyrate. The reactions were performed at 0.5 μM YbtT and varying concentrations of the designated substrate. The *p*-NP acetate data were fit to the Michaelis-Menten equation ($R^2 = 0.9914$), and the calculated kinetic parameters are reported in Table 2; mean of $n = 3$ with standard error plotted. *C,* time courses of YbtT-catalyzed hydrolysis of the esterase substrate, *p*-NP acetate, and a protease substrate, glycine *p*-nitroanilide. All data have been normalized to account for spontaneous background hydrolysis of the substrates in the absence of enzyme. All reactions were performed with 0.5 μM enzyme and 1 mM substrate. PMSF treatment was performed at 1 mM. Mean of $n = 3$ for all conditions except YbtT with glycine *p*-nitroanilide and YbtT + PMSF with *p*-NP acetate, where $n = 2$. Standard deviation plotted.

Table 2
Kinetic parameters for YbtT hydrolysis of *p*-NP ester substrates

Substrate	k_{cat}	K_m	k_{cat}/K_m
	min^{-1}	mM	$_M^{-1}$ s^{-1}
p-NP acetate (—CH_3)	2.25 ± 0.09	1.5 ± 0.1	25.3 ± 2.1
p-NP butyrate (—$CH_2CH_2CH_3$)			20.5[a]

[a] Because experiments with *p*-NP butyrate were limited by the substrate's solubility, a full Michaelis-Menten analysis could not be performed. The k_{cat}/K_m value reported was estimated from the reaction progress curve, as described by Copeland (56).

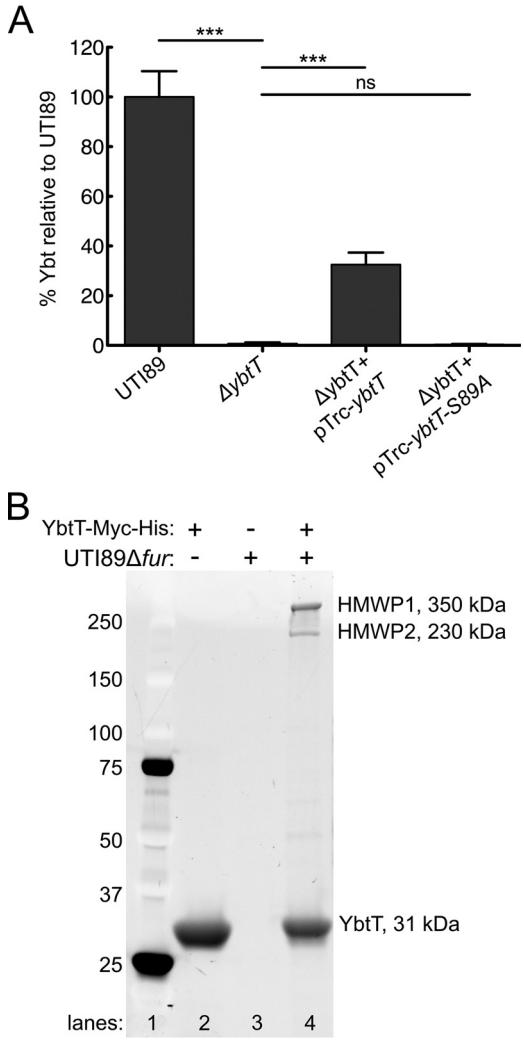

Figure 5. YbtT enzymatic activity is important for optimal Ybt production, and it forms a complex with Ybt biosynthetic proteins. *A,* Ybt levels, quantified by stable isotope dilution and LC-MS/MS, of UTI89, Δ*ybtT*, and Δ*ybtT* strains complemented with either WT *ybtT* or catalytically inactive *ybtT-S89A* cloned into the plasmid pTrcHis2. Strains were grown under iron-restricted conditions. Mean of $n = 3$ with standard deviation plotted, one-way ANOVA compared with multiple comparison post-test to Δ*ybtT*; ***, $p < 0.0001$; *ns*, $p > 0.05$. *B,* SYPRO Orange-stained SDS-polyacrylamide gel of *in vitro* pulldown experiment with YbtT loaded onto nickel beads and exposed to UTI89Δ*fur* cellular lysate (*lane 4*). Additional sets of beads were exposed to either YbtT only (*lane 2*) or lysate only (*lane 3*) as negative controls. Molecular mass markers (*lane 1*) are indicated on the *left* in kDa. YbtT specifically pulled down two proteins, which were identified as HMWP1 and HMWP2 by LC-MS/MS.

TEIIs (17). These results are consistent with the hypothesized role for the serine hydrolase catalytic triad in YbtT hydrolase activity.

Catalytically active YbtT restores Ybt production in a ybtT deletion mutant

Previous work has demonstrated that *ybtT* deletion mutants in *Y. pestis* and UPEC are deficient in Ybt production (12–14). To further investigate the role of *ybtT* in UPEC, we used the model UPEC strain UTI89 and expressed plasmid-encoded YbtT in UTI89Δ*ybtT* and monitored Ybt production by LC-MS/MS. Expression of WT *ybtT*, but not catalytically inactive *ybtT-S89A*, partially restored Ybt production in UTI89Δ*ybtT*

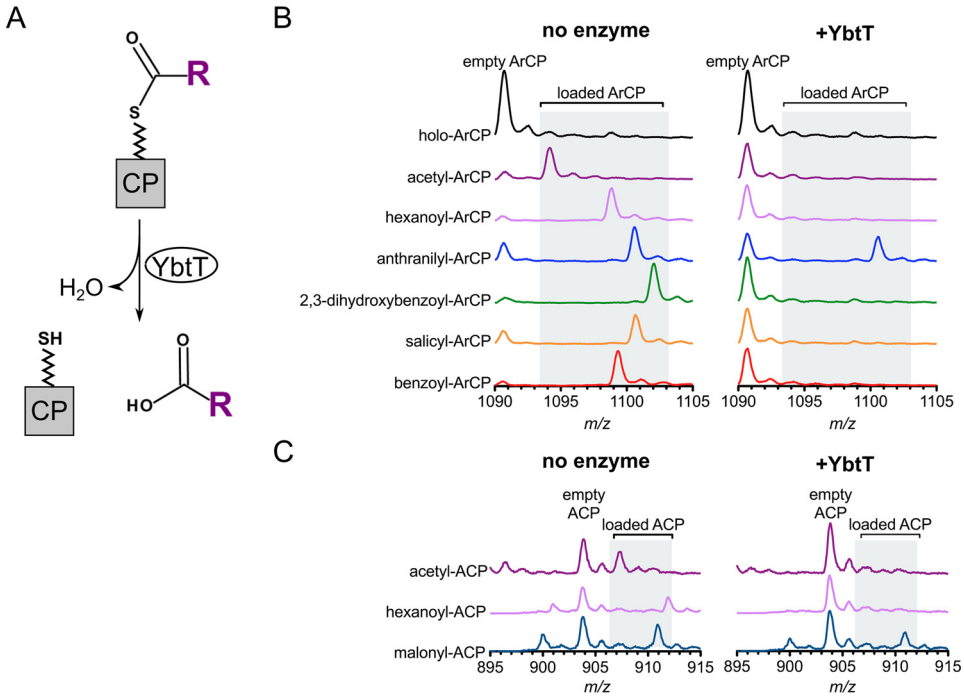

Figure 6. MS-based assessment of YbtT's substrate specificity for acylated CP domains. *A,* reaction scheme of YbtT-catalyzed hydrolysis of small molecules from phosphopantetheinylated CP domains. *B* and *C,* mass spectra of the +12 charge state of holo-ArCP (*B*) and holo-ACP (*C*) that had been loaded with candidate small molecule substrates and incubated for 30 min with or without 1 μM YbtT (*right* and *left*, respectively).

(Fig. 5*A*). Differences in Ybt expression were not attributable to growth defects, as all strains grew to the same extent (Fig. S3). These results suggest that although *ybtT* is not essential for bacterial growth in culture, its serine catalytic triad plays an important role in maximizing Ybt production.

YbtT interacts with HMWP1 and HMWP2

TEIIs hydrolyze thioester bonds that tether small molecules to phosphopantetheinylated CPs. In addition to Ybt biosynthetic enzymes, UTI89 can also express phosphopantetheinylated enzymes involved in enterobactin, fatty acid, and colibactin biosynthesis (31). To identify YbtT-interacting proteins, we performed pulldown assays with recombinantly purified YbtT. Because expression of YbtT and other phosphopantetheinylated enzymes are subject to transcriptional repression by the Fur transcription factor, we hypothesized that YbtT-binding partners would be enriched in prey lysates from a *fur* deletion mutant. YbtT was therefore exposed to UTI89Δ*fur* prey lysates, and the eluates were analyzed by SDS-PAGE. Two exceptionally high-molecular-weight proteins were specifically pulled down by YbtT (Fig. 5*B*). In-gel trypsin digest and mass spectrometric analysis of the peptides revealed these proteins as HMWP1 (350 kDa) and HMWP2 (230 kDa), the major Ybt NRPS/PKS biosynthetic proteins. No other phosphopantetheinylated enzymes were detected in the pulldown. These results are consistent with HMWP1 and HMWP2 as interacting partners of YbtT.

YbtT hydrolyzes ppant thioesters of the HMWP2 aryl carrier domain

We next sought to determine whether YbtT hydrolyzes ppant thioesters on HMWP2. We expressed the aryl carrier protein domain (ArCP), the first phosphopantetheinylated domain of HMWP2 (amino acids 1–100) and the site of salicylic acid loading, and we enzymatically generated both aromatic and aliphatic thioesters. Their identity was confirmed by full scan LC-MS and the ppant ejection method (LC-MS/MS) (32, 33). Our panel of test substrates included the salicyl thioester of ArCP, which is a canonical intermediate of Ybt biosynthesis. After incubating each substrate with YbtT for 30 min, we used LC-MS to detect thioester bond hydrolysis. Complete conversion to the empty holo-ArCP product was observed for both aromatic and aliphatic thioesters except anthranilyl-ArCP, which was only partially hydrolyzed (Fig. 6*B*). Hydrolysis of this chemically diverse ppant thioester series, which includes the canonical salicyl thioester intermediate, is consistent with broad substrate specificity for YbtT.

YbtT hydrolyzes multiple aliphatic thioesters of the HMWP1 acyl carrier domain

To determine whether YbtT also hydrolyzes ppant thioesters on HMWP1, we prepared thioesters of phosphopantetheinylated ACP from the HMWP1 PKS module (amino acids 1813–1995). Here, we were limited to enzymatic synthesis of acetyl-, hexanoyl-, and malonyl-ACP thioesters. YbtT thioesterase activity with each ACP substrate was monitored by LC-MS, as described for ArCP above. YbtT hydrolyzed the short and medium length acyl chains but not malonyl-ACP, a carboxylated acyl chain and a canonical Ybt biosynthetic precursor (Fig. 6*C*). These results demonstrate that phosphopantetheinylated CPs necessary for both early (HMWP2) and late (HMWP1) Ybt biosynthesis may be YbtT substrates. The reduced activity on malonyl-ACP, relative to the other structurally related thioes-

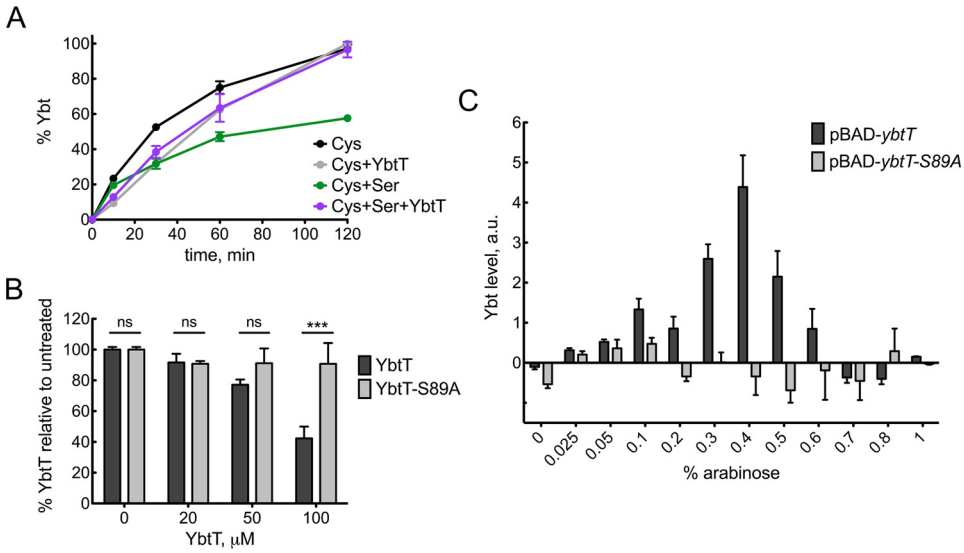

Figure 7. YbtT edits Ybt biosynthesis *in vitro,* and its expression must be regulated *in vivo.* *A,* time course of Ybt accumulation during full *in vitro* reconstitution in the presence of the cognate substrate, Cys, and the noncognate substrate, Ser, with or without YbtT. Ybt levels are expressed as a percent relative to the level reached in the Cys condition (*black*) at 120 min. Mean of $n = 3$ with standard deviation plotted. *B,* Ybt accumulation during full *in vitro* reconstitution in the presence of increasing concentrations of YbtT or YbtT–S89A. Ybt levels were measured at 10 min and are expressed as a percent relative to the 0 μM control. Mean of $n = 3$ with standard error plotted, one-way ANOVA compared with multiple comparison post-test; ***, $p < 0.0001$; *ns*, $p > 0.05$. *C,* Ybt levels when the isogenic mutant UTI89Δ*ybtT* was transformed with either pBAD-*ybtT* or pBAD-*ybtT-S89A* and grown under iron-restricted conditions in the presence of increasing concentrations of arabinose to induce expression of *ybtT* or *ybtT-S89A*. To account for the effects of arabinose, all of the data were normalized by subtracting the Ybt levels of a vector-only control (pBAD) treated with the same concentrations of arabinose. Mean of $n = 3$ with standard error plotted.

ters, suggests some degree of YbtT substrate selectivity that acts to spare the canonical precursor from hydrolysis.

YbtT increases Ybt biosynthesis in the presence of a noncanonical precursor

To determine how YbtT directly affects Ybt biosynthesis, we added it to the *in vitro* reconstituted system developed by Miller *et al.* (3), where no effect was observed with YbtT at 10-fold excess over the other enzymes. The four essential enzymes for Ybt biosynthesis, YbtE, HMWP2, HMWP1, and YbtU, were purified and combined with the canonical precursors: salicylic acid, L-cysteine, and malonyl-CoA. We found that L-serine, a physiologically plausible, noncanonical precursor that structurally mimics L-cysteine, inhibited Ybt production during *in vitro* biosynthesis (Fig. 7*A*). In the presence of competing L-serine, YbtT addition at 10-fold excess over the other enzymes restored the final Ybt yield to that observed in the absence of L-serine. These observations suggest that YbtT edits Ybt biosynthetic intermediates, preventing HMWP2 and HMWP1 inactivation by misincorporated L-serine thioesters that would otherwise irreversibly inhibit the biosynthetic pathway.

YbtT diminishes the rate of Ybt biosynthesis

YbtT slowed the initial rate of Ybt production in both the presence and absence of L-serine (Fig. 7*A*). Given the observed low substrate specificity of YbtT, we hypothesized that this is attributable to hydrolysis of productive, canonical thioester intermediates. Indeed, when only canonical Ybt precursors were made available to biosynthetic proteins, increasing YbtT concentrations progressively diminished Ybt production (Fig. 7*B*) to a degree (~20% lower yield with 50 μM YbtT) that may not have been evident in the previous analysis (3). These findings suggest that, whereas YbtT may maintain biosynthetic activity by removing nonproductive thioesters from HMWP2 and HMWP1, its low-specificity counterproductively can also reduce Ybt production by hydrolyzing canonical Ybt precursors.

High in vivo YbtT expression diminishes Ybt production

Given that increasing YbtT concentrations can diminish *in vitro* Ybt biosynthesis, we hypothesized that physiological YbtT expression must be optimized to balance hydrolysis of nonproductive thioesters with removal of productive, canonical Ybt precursors from HMWP1 and HMWP2. To test this hypothesis, we genetically complemented UTI89Δ*ybtT* with a *ybtT* expression vector under tight control by an arabinose-inducible promoter. YbtT expression in arabinose-supplemented medium was confirmed by Western blotting (data not shown). In an iron-restricted medium with increasing arabinose concentrations, Ybt levels increased up to an arabinose concentration of 0.4% and decreased at concentrations exceeding 0.4% (Fig. 7*C*). In contrast, increasing expression of the inactive mutant $ybtT^{S89A}$ did not affect Ybt production (Fig. 7*C*). These data are consistent with the existence of a cellular YbtT expression level at which competing productive and nonproductive thioester hydrolysis rates lead to optimal Ybt production.

Structural comparison of YbtT to human TEII

Our results indicate that YbtT is required for optimal Ybt production; hence, YbtT inhibition represents a candidate therapeutic strategy for enterobacterial infections. To investigate whether selective inhibition of this bacterial thioesterase is feasible, we carried out initial structural analysis comparing YbtT to human TEII (hTE2) (Fig. 8). The core hydrolase folds for YbtT and hTE2 are very similar, with the major difference being in the conformation of the structurally dynamic lid sub-

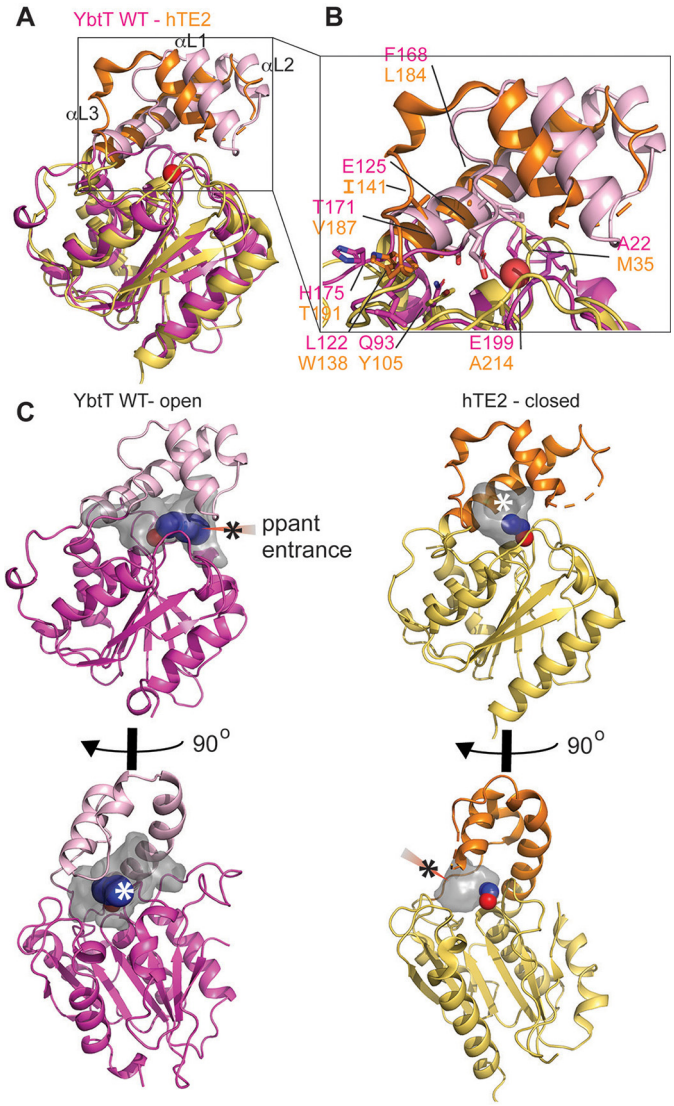

Figure 8. Comparison of YbtT to human TEII. *A,* overlay of crystal structures YbtT WT (*magenta*) with human thioesterase II (hTE2, *orange/gold*, PDB code 4XJV). α-Helices that compose the lid subdomain are labeled and colored *orange* in hTE2. Position of the active site is denoted by the water occupying the oxyanion hole (*red sphere*). *B,* comparison of structurally equivalent residues that line the putative active site and inhibitor pockets of YbtT and hTE2. Residues labeled vary the most in either size, polarity, or charge between the two structures. *C,* comparison of ppant cavities and entrance tunnels analyzed using CAVER, with coloring and labeling as in Fig. 3*B*. Cavity volumes calculated by CAVER are YbtT = 756 Å^3 and hTE2 = 128 Å^3.

domains (Fig. 8*A*). The YbtT lid subdomain is in the open configuration, whereas the hTE2 structure is in a closed conformation, with the lid subdomain collapsed onto the active site (26). This difference is indicated by the active-site cavity volumes (YbtT = 756 Å^3; hTE2 = 128 Å^3) (Fig. 8*C*). Comparisons of the active-site cavities also indicate several differences in side chain size, chemical nature, and charge between YbtT and hTEII in the putative binding region for competitive inhibitors (Fig. 8*B*). These observations suggest that YbtT-specific inhibitors with decreased or little potency against hTE2 could be designed.

Discussion

In this study, we report the first structural and biochemical characterization of YbtT, a TEII required for maximal *in vivo* Ybt production, but unnecessary for maximal *in vitro* reconstitution. Structural, biochemical, and bacterial culture studies suggest that YbtT helps maintain HMWP1 and HMWP2 activity through a relatively nonspecific thioesterase activity that removes nonproductive, inhibitory thioesters aberrantly incorporated into the Ybt biosynthetic pathway during bacterial growth. YbtT slowly hydrolyzes a variety of productive and erroneous molecules from HMWP1 and HMWP2 CP domains. The resulting free NRPS/PKS ppant thiols can then resume Ybt biosynthesis. This is exemplified by YbtT-mediated restoration of *in vitro* biosynthesis in the presence of a nonproductive precursor molecule.

Two models have been proposed for TEII editing of NRPS/PKS pathways, specifically pertaining to the enzyme's substrate specificity at the level of the hydrolyzed small molecule (15, 17, 25). In the high-specificity model, the TEII specifically recognizes noncognate precursors attached to CPs and hydrolyzes these with high-catalytic efficiency. In the low-specificity model, TEII hydrolyzes both cognate and noncognate precursors from CPs with low-catalytic efficiency. This low-specificity model can be tolerated because flux through the pathway greatly exceeds nonspecific hydrolysis or because cognate precursors are more strongly bound to the NRPS/PKS, shielding them from hydrolysis.

The substrate profiling, *in vitro* reconstitution, and *in vivo* overexpression results for YbtT are consistent with the low-specificity editing model for Ybt biosynthesis. In cultured *E. coli*, this is suggested by diminished Ybt production when YbtT expression increases beyond an optimal level. During *in vitro* reconstituted biosynthesis, the low-specificity model is supported by diminished Ybt production upon YbtT addition at >10-fold excess (100 μM) and at longer time points in the presence of only cognate precursors. The catalytic efficiency (k_{cat}/K_m) of YbtT on *p*-NP acetate and butyrate was quite low, although it is possible that it would be more active on other *p*-NP ester substrates or other thioester substrates, such as acyl-CPs. YbtT hydrolyzed both productive and nonproductive precursors to Ybt at the ArCP domain, including aromatic and short acyl groups, with only a few exceptions. It was active on salicylic acid, a correct building block of Ybt but not anthranilic acid. It may be that replacing the 2-hydroxyl of salicylic acid with an amino group, as in anthranilic acid, sterically hinders substrate binding by YbtT. The ability of YbtT to hydrolyze 2,3-dihydroxybenzoyl-ArCP (a misincorporated enterobactin biosynthetic intermediate) and to reverse L-serine-mediated inhibition of Ybt biosynthesis is consistent with a role for YbtT in removing physiologically relevant misincorporation errors (34, 35). YbtT can thus hydrolyze both productive and nonproductive intermediates at NRPS CP domains.

In contrast to its mode of action at the pathway level, YbtT activity at the PKS CP domain was more consistent with the high-specificity editing model, avoiding malonyl thioester hydrolysis but readily hydrolyzing nonproductive acetyl and hexanoyl thioesters. Similar PKS CP domain specificity was observed in RifR and tylosin TEII, where substrate selectivity was attributed to the absence of a terminal carboxyl group (17, 25). Acetyl thioesters may arise by spontaneous decarboxylation of malonyl thioesters. They may also arise during post-

translational modification of NRPS/PKSs through utilization of an acetyl-CoA, rather than a free CoA, by the ppant transferase (34). Nevertheless, low-specificity hydrolysis at other CP domains likely dominates the overall picture during Ybt biosynthesis, and YbtT acts as a low-specificity editor. It is possible that YbtT inactivity on malonyl-CP is a retained, vestigial function of an ancestral TEII that subsequently evolved with the biosynthetic pathway to edit NRPS domains. It remains to be determined whether the ability of YbtT to spare malonyl thioesters is due to the identity of the small molecule, the identity of the CP domain, or a combination of both. Overall, our data suggest that low-specificity editing of a multi-CP domain biosynthetic pathway may conceal high-specificity editing at specific CP domains. It also suggests that the low-specificity model of editing may be a useful strategy for TEIIs that edit hybrid NRPS/PKS pathways with many structurally unique precursors, such as the Ybt biosynthetic pathway.

The crystal structures of YbtT provide a structural explanation for the observed substrate specificity. Previous structural and functional characterizations of RedJ (22) and RifR (25) have noted that the chemical nature of residues in the lid subdomain lining the active-site substrate pocket correlate with substrate specificities. Specifically, this region of RedJ is rich in hydrophobic side chains, which would favor binding to the long-chain acyl thioesters that are the preferred substrates for this enzyme (22). In contrast, the same region of RifR contains more polar side chains, and correspondingly, RifR exhibits lower substrate specificity (25). Our YbtT structure, like that of RifR, also contains several polar and charged side chains in this region, consistent with the low substrate specificity we observe. Our structures also reveal that YbtT crystallized with the lid subdomain in an open conformation that may be stabilized by crystal contacts, based on low relative B-factors. Such a conformation in solution would suggest ready access to the active site and, hence, fast enzyme kinetics. However, YbtT displayed slow enzyme kinetics. Previous crystallographic studies have noted multiple conformations for the lid subdomain of TEIIs and TEIs with this fold (22, 36). In addition, solution studies by NMR indicate dynamics between the open and closed lid subdomain conformations (27, 37). Our kinetics results are supportive of these previous observations, and access to the YbtT active site may be controlled by the conformational dynamics. Additionally, structural comparison to hTE2 shows that the YbtT active-site pocket contains some vastly contrasting features, suggesting that specific inhibition of YbtT might be achieved without potently inhibiting hTE2.

The results of the pulldown with purified YbtT suggest that this TEII interacts with HMWP1 and HMWP2 but not other phosphopantetheinylated proteins in *E. coli*. There are few reports on the protein–protein interactions between TEIIs and the NRPSs and PKSs on which they act. EntH, the TEII from enterobactin biosynthesis, was shown to interact with an ArCP on one of the pathway's NRPSs in a bacterial two-hybrid experiment (38). The TEII involved with surfactin biosynthesis was shown to bind a CP by NMR, and binding was enhanced when the CP was phosphopantetheinylated and loaded with a small molecule, although it should be noted that the CP that was used did not come from the same biosynthetic pathway (27). Our pulldown does not tell us whether YbtT is primarily interacting with either HMWP1 or HMWP2, and it does not tell us precisely how these proteins interact, so this is an area for future research. Our acyl-CP activity data do suggest that YbtT may bind the ArCP and ACP domains because YbtT could hydrolyze small molecules from both. If TEIIs are scanning their cognate NRPSs and PKSs, then these protein–protein interactions may be very low affinity and difficult to quantify with standard protein-binding techniques (39). The application of MS to study TEII activity on CPs, as applied in this study, is very revealing and further investigation of protein–protein interactions may build upon this approach to understand the molecular mechanisms behind TEII substrate specificity for CP domains.

Experimental procedures

Bacterial strains, culture conditions, and plasmid construction

The cystitis-derived UPEC model strain UTI89 was used in this study (40, 41). The creation of the isogenic mutant UTI89Δ*ybtT* was previously described (14). UTI89Δ*fur* was generated using the Lambda Red recombinase method, and the antibiotic cassette was subsequently removed (42). For growth in iron-restricted conditions, strains were first grown for ~18 h in Luria-Bertani (LB) broth (BD Biosciences) at 37 °C under rotating conditions. These cultures were then inoculated 1:1000 into M63 minimal media supplemented with 0.2% (v/v) glycerol and 10 mg/ml niacin (Sigma) and grown at 37 °C under rotating conditions for ~18 h. Ampicillin (100 μg/ml, Goldbio) was used for plasmid selection, where appropriate. Arabinose was added at inoculation to induce YbtT and YbtT–S89A expression during the 18-h M63 growth in the YbtT overexpression study.

Plasmids for YbtT expression studies and protein purification were constructed using the vector backbones pTrcHis2 (Invitrogen) and pBAD/Myc-His (Invitrogen) and standard molecular biology techniques, including PCR and the restrictions enzymes NcoI and HindIII (New England Biolabs). The S89A and H225A mutants were generated with a standard site-directed mutagenesis kit (Quikchange, Agilent). pET22b-ArCP and pET22b-YbtU were constructed as described previously (3, 43). YbtE was cloned into a pET28a vector with an N-terminal His_6 tag using NdeI and XhoI restriction sites. YbtT, ArCP, YbtU, and YbtE were all cloned from the UTI89 genome. All other plasmids for ACP, Sfp, HMWP1, and HMWP2 expression were kind gifts from Dr. Tim Wencewicz and the Walsh strain collection.

Recombinant protein expression and purification

pTrcHis2 expression plasmids of YbtT, YbtT–S89A, YbtT–D197A, and YbtT–H225A with a C-terminal Myc (EQKLISEEDL)-His_6 tag were expressed in the BL21(DE3) *E. coli* strain. The expression strains were grown overnight in LB at 37 °C, and then back-diluted 1:50 into 3 liters of LB supplemented with 100 μg/ml ampicillin. The cultures were grown at 37 °C to OD 0.4–0.6 and then induced with 1 mM isopropyl β-D-thiogalactopyranoside (IPTG, Goldbio) for 4 h at 37 °C. The cells were resuspended in lysis buffer (20 mM Tris (pH 8.0), 300 mM NaCl,

5 mM β-mercaptoethanol, 5 mM imidazole) at a ratio of 10 ml of buffer to 1 liter of culture and then stored at −80 °C.

For YbtT, YbtT–S89A, YbtT–D197A, and YbtT–H225A purification, the resuspended cell pellets were thawed; rotated for 30 min at room temperature with 1 mg/ml lysozyme (Sigma), 2 μg/ml DNase I (Sigma), and 2 mM $MgSO_4$; and sonicated. The lysate was isolated by centrifugation at 12,000 × *g* for 1 h at 4 °C (Beckman Coulter); filtered through a 0.44-μm filter (Millipore); run over a column of Ni-NTA–agarose beads (Goldbio); and washed with 20 mM Tris (pH 8.0), 300 mM NaCl, 5 mM β-mercaptoethanol, 20 mM imidazole; and the protein was eluted with 20 mM Tris (pH 8.0), 300 mM NaCl, 5 mM β-mercaptoethanol, 300 mM imidazole. The elutions were pooled, concentrated in a 10-kDa cutoff Vivaspin 20 concentrator (Sartorius), and further purified on a 16/600 Superdex 75 pg gel filtration column (GE Bio-Sciences) equilibrated with running buffer (50 mM potassium phosphate (pH 7.4, Sigma), 100 mM KCl (Sigma), 2 mM tris(2-carboxyethyl)phosphine hydrochloride (TCEP, Goldbio)). In the case of YbtT–D197A, the running buffer contained 300 mM KCl. Fractions containing YbtT or the respective mutant were confirmed by SDS-PAGE and Coomassie Blue staining, pooled, concentrated in a 10-kDa cutoff Vivaspin 20 concentrator, and dialyzed into storage buffer (50 mM potassium phosphate (pH 7.4), 100 mM KCl, 2 mM TCEP, 10% glycerol) overnight at 4 °C in a 3-ml 2000 MWCO dialysis cassette. After dialysis, proteins were flash-frozen and stored at −80 °C.

For YbtE purification, the expression vector was transformed into Rosetta D3 *E. coli* cells. The cells were grown at 37 °C to an OD ~1.0 and then induced with 250 mM IPTG for 5 h at 30 °C. Cells were pelleted and resuspended in 150 mM NaCl, 10 mM Tris (pH 8.5), 50 mM K_2HPO_4, 5 mM imidazole, and 10 mM β-mercaptoethanol supplemented with lysozyme and DNase. They were lysed by sonication, and the debris was pelleted by centrifugation for 30 min at 16,000 × *g*. The supernatants were passed over Ni-NTA super flow resin (Qiagen); washed with 300 mM NaCl, 20 mM imidazole, and 50 mM K_2HPO_4 (pH 8.0); and then eluted in 300 mM NaCl, 250 mM imidazole, and 50 mM K_2HPO_4 (pH 8.0). Eluted protein was further purified by size-exclusion chromatography on a Superdex 16/600 S75 column (GE Bio-Sciences) in 20 mM HEPES and 150 mM NaCl with 1 mM dithiothreitol (DTT).

Purification of ArCP and ACP in their apo and holo states was performed as described previously (43, 44). Purification of Sfp was also performed as described previously (45). HMWP2, HMWP1, and YbtU were expressed and purified as described previously, with minor modifications (3, 46, 47).

For HMWP2 purification, the BL21(DE3) *E. coli* strain expressing pHMWP2.CH8 was grown in 2× YT broth containing 2 mM $MgCl_2$ at 37 °C to OD 0.4, then moved to 16 °C, and at OD 0.8 induced with 50 μM IPTG for 16 h at 16 °C. For HMWP1 purification, the BL21(DE3) *E. coli* strain expressing pET28b–HMWP1 was grown in LB at 37 °C to OD 0.6, and then induced with 75 μM IPTG for 16 h at 16 °C. For both proteins, the cells were resuspended in lysis buffer (20 mM Tris (pH 8.0), 500 mM NaCl, 5 mM β-mercaptoethanol, 1 mM phenylmethylsulfonyl fluoride (PMSF, Sigma), EDTA-free protease inhibitor mixture tablet (SIGMA*FAST*™), 5 mM imidazole) at a ratio of 15 ml of buffer to 1 liter of culture and then stored at −80 °C. The lysates were obtained as described above and incubated in batch with Ni-NTA–agarose beads overnight at 4 °C. The beads were then packed into a column and washed with buffer (20 mM Tris (pH 8.0), 500 mM NaCl, 5 mM β-mercaptoethanol, 1 mM PMSF) containing 5 mM imidazole and 20 mM imidazole, sequentially; and the protein was eluted with buffer and a gradient from 30 to 100 mM imidazole. All steps were performed at 4 °C. The elutions containing HMWP2 or HMWP1 were pooled, concentrated in a 100,000 concentrator (Amicon), and further purified on a Mono Q HR 5/5 anion-exchange column (GE Healthcare) with running buffer A (20 mM Tris (pH 8.0), 5 mM β-mercaptoethanol) and running buffer B (20 mM Tris (pH 8.0), 1 M NaCl, 5 mM β-mercaptoethanol). Fractions containing the target protein were analyzed, concentrated, dialyzed into storage buffer (25 mM Tris (pH 8.0), 2 mM TCEP, 10% glycerol), flash-frozen, and stored at −80 °C, as described above.

For YbtU, the BL21(DE3) *E. coli* strain expressing pET22b-YbtU was grown at 22 °C without IPTG induction for 24 h and resuspended in lysis buffer described for HMWP2 and HMWP1. YbtU was purified over Ni-NTA as described for YbtT, except 500 mM NaCl was included in all buffers. It was further purified on a 16/600 Superdex 200 pg gel-filtration column (GE Bio-Sciences) in 20 mM Tris (pH 8.0), 500 mM NaCl, 5 mM β-mercaptoethanol. The storage buffer contained 25 mM Tris (pH 8.0), 100 mM NaCl, 2 mM TCEP, 10% glycerol.

Crystallization, data collection, and structure determination

For crystallization, YbtT and YbtT–S89A were purified as described above and concentrated to 15 or 17 mg/ml for WT and S89A, respectively, in 20 mM HEPES (pH 7.4), 150 mM NaCl, and 1 mM DTT. Crystals of WT and S89A YbtT were obtained by mixing the concentrated protein solution with reservoir solution (either 200 mM tri-sodium citrate, 21% PEG 3350, 0.5% *n*-dodecyl-β-D-maltoside (S89A) or 200 mM di-ammonium hydrogen citrate, 20% PEG 3350 (WT)) in a 1:1 ratio. Crystals routinely formed over the course of 2–4 days. Crystals were cryoprotected in reservoir solution supplemented with 20% ethylene glycol and stream-frozen at 100 K. X-ray diffraction data were collected at the Advanced Light Source beamline 4.2.2 at Lawrence Berkeley National Laboratory. Crystals contained one molecule in the asymmetric unit with 43% solvent content. Data were processed using XDS (48). Data collection and refinement statistics are given in Table 1.

The phase problem was solved by molecular replacement in the program PHASER (49) using a polyalanine model of the *S. coelicolor* thioesterase RedJ (PDB code 3QMW (22)). Following rigid body refinement, the model was built by a combination of auto-rebuilding with PHENIX (50) using RESOLVE (51) and manual building in COOT (52). WT and S89A YbtT were refined against data to 1.9 and 1.4 Å, respectively, using PHENIX. Hydrogens were generated in the final stages of refinement and included as a riding model. The final model for both WT and S89A consisted of residues 1–248. All residues are within the most favored (98.0/97.6%) and additional allowed regions (2.0/2.4%) of a Ramachandran plot. Molprobity scores were 1.08/1.00, and clash scores were 2.86/2.08 for the

final models of WT/S89A YbtT, respectively. Molecular graphics figures were created using PyMOL. All crystallographic and analysis software used were compiled and distributed by the SBGrid resource (53), and diffraction images were archived with the SBGrid Data Bank (54). The coordinates and experimental structure factors of WT and S89A have been deposited in the RCSB Protein Data Bank and assigned the PDB codes 6BA8 and 6BA9, respectively.

p-NP acetate, *p*-NP butyrate, and glycine *p*-nitroanilide activity assays

Enzymatic assays were performed as described previously (17, 30). All substrates were from Sigma. Reactions were performed in 1-ml cuvettes at 30 °C in 50 mM potassium phosphate (pH 7.4). All reactions contained 5% DMSO (v/v), as it was the vehicle for solubilizing the substrates. YbtT and mutants were used at 0.5 μM, and substrates were used at variable concentrations in excess of enzyme. All reaction components except substrate were pre-incubated at 30 °C for 5 min to reach temperature, and then the reactions were initiated by adding substrate and mixing. Time courses with *p*-NP acetate and *p*-NP butyrate were collected by monitoring absorbance at 405 nm, and the product concentration was calculated with $\epsilon = 18{,}000\ \text{M}^{-1}\ \text{cm}^{-1}$ (manufacturer's protocol). Time courses with glycine *p*-nitroanilide were collected by monitoring absorbance at 405 nm, and the product concentration was calculated with $\epsilon = 9500\ \text{M}^{-1}\ \text{cm}^{-1}$ (55). Data were corrected for background spontaneous hydrolysis in the absence of enzyme. Analysis was performed with GraphPad Prism 4 (GraphPad Software). Because *p*-NP-butyrate had limited solubility and saturation could not be reached, a full Michaelis-Menten analysis could not be performed. The k_{cat}/K_m value reported was estimated from the reaction progress curve, as described by Copeland (56).

Ybt detection in bacterial culture

Ybt was detected in spent supernatants by stable isotope dilution after growth under iron-restricted conditions. A ^{13}C-Ybt internal standard was prepared by growing UTI89 in M63 minimal media supplemented with 0.2% (v/v) $^{13}C_3$-glycerol (Sigma) and 10 mg/ml niacin, as described previously (2). After bacterial growth, 25 μl of ^{13}C-Ybt internal standard (4) and 6 μl of 0.5 M $FeCl_3$ were added to 1 ml of culture supernatant. The samples were extracted on C18 silica columns (United Chemical Technologies) with 80% methanol (Sigma). Ybt was detected using a multiple reaction monitoring method on a Shimadzu Prominence UFLC-coupled AB Sciex QTrap 4000 mass spectrometer with a Turbo V electrospray ionization source. The LC separation was performed with an Ascentis Express phenyl–hexyl column (100 × 2.1 mm, 2.7 μM; Sigma) and the mobile phases: A = HPLC-grade water + 0.1% (v/v) formic acid (Sigma) and B = 90% acetonitrile (EMD Millipore) + 0.1% (v/v) formic acid. All LC and MS settings were the same as described previously (57). Ybt levels were assessed by taking the peak area ratio of the native isotope Fe–Ybt to the internal standard Fe–^{13}C-Ybt.

Pulldown and protein identification by LC-MS/MS

The UTI89Δ*fur* lysate was obtained by growing the strain at 37 °C overnight; back-diluting it into 1 liter of fresh LB and growing at 37 °C shaking for 18 h; pelleting the cells at 8000 rpm for 10 min, 4 °C (Beckman Coulter); discarding the supernatant; resuspending the cell pellet in 10 ml of loading buffer (20 mM Tris (pH 8.0), 300 mM NaCl, 5 mM β-mercaptoethanol, 10 mM imidazole); and freezing the resuspension at −80 °C. After thawing the cell pellet, it was lysed and clarified as described for protein purification, with the exception that an additional 30 ml of lysis buffer was added after treatment with lysozyme and DNase I but prior to sonication. Three mini-spin columns were prepared with a 50-μl bed volume of Ni-NTA beads. Two of these columns were loaded with 0.5 mg of purified YbtT–Myc–His, and one was mock-treated with YbtT storage buffer (described above) to serve as a prey-only control. Loading of YbtT (bait) was performed by rotating the columns for 15 min at 4 °C. Excess bait was washed away with 500 μl of loading buffer. 1500 μl of UTI89Δ*fur* lysate (prey) was added to one YbtT-loaded column and the mock-treated column. The remaining YbtT-loaded column was treated with 1500 μl of loading buffer as a bait-only control. The columns were rotated at 4 °C overnight and washed twice with 500 μl of YbtT wash buffer (see above), and protein complexes were eluted with 100 μl of YbtT elution buffer (see above). The elutions from the three columns were analyzed by SDS-PAGE and SYPRO Orange staining according to the manufacturer's protocol (Sigma).

To identify the proteins pulled down by YbtT, the gel bands at 250 and >250 kDa were excised and digested with trypsin overnight. The extracted peptides were dried down and redissolved in 10 μl of 5% acetonitrile, 0.1% formic acid. 5 μl were injected and run on an LTQ-Orbitrap Velos Pro using a 1-h gradient on a Dionex RSLCnano HPLC with a 0.075 × 250-mm C18 Waters CSH130 1.7-μm, 130 Å column. All MS/MS samples were analyzed using Mascot (Matrix Science, London, UK; version 2.5.0). Mascot was set up to search the NCBInr database (selected for *E. coli*, 1,210,071 entries) assuming the digestion enzyme trypsin. Mascot was searched with a fragment ion mass tolerance of 0.60 Da and a parent ion tolerance of 10.0 ppm. Deamidation of asparagine and glutamine, oxidation of methionine, carbamidomethyl of cysteine, and phosphopantetheinylation of serine were specified in Mascot as variable modifications. Scaffold (version Scaffold_4.4.0, Proteome Software Inc., Portland, OR) was used to validate MS/MS-based peptide and protein identifications. Peptide identifications were accepted if they could be established at greater than 80.0% probability by the Scaffold local false discovery rate algorithm. Protein identifications were accepted if they could be established at greater than 99.0% probability and contained at least two identified peptides.

ArCP and ACP acylation

Protocols for enzymatic acylation of CPs were developed from past reports (43, 58, 59). Reactions were performed in 50 mM potassium phosphate (pH 7.4) + 100 mM KCl. ArCP acylation reactions performed with YbtE included: 1 μM YbtE, 500 μM aryl

acid, 10 mM $MgCl_2$, 2 mM TCEP, 1 mM ATP, and 25 μM holo-ArCP. ArCP and ACP acylation reactions performed with Sfp included: 1 μM Sfp, 20 μM acyl-CoA, 10 mM $MgCl_2$, 2 mM TCEP, and 20 μM apo-ACP or ArCP. All reactions were incubated for 2 h at 37 °C, and then excess substrate was removed with 7K Zeba desalting columns (ThermoFisher Scientific). The acylation was confirmed by full scan LC-MS (instrument details above) to obtain a deconvoluted observed molecular weight (Analyst and MagTran) and by the ppant ejection method (32, 33).

LC-MS-based YbtT assay on ArCP and ACP

Activity assays were performed in a 100-μl reaction volume with 20 μM acyl-CP substrate and 1 μM YbtT (or YbtT storage buffer as a negative control) in 50 mM potassium phosphate (pH 7.4) + 100 mM KCl + 2 mM TCEP. The reactions were incubated for 30 min at 37 °C. The samples were diluted 1:2 with 100 mM ammonium bicarbonate and immediately analyzed by LC-MS (instrument details above) in a positive ion mode with an enhanced resolution scan centered on the +12 charge state of the protein.

Ybt in vitro reconstitution

A solution of 5 μM YbtE, 5 μM HMWP2, 5 μM HMWP1, 5 μM YbtU, 0.5 μM Sfp, 100 mM Tris (pH 8.0), 10 mM $MgCl_2$, 1 mM TCEP, 100 μM CoASH, 2 mM L-cysteine, 0.75 mM SAM, 0.75 mM NADPH, 1 mM malonyl-CoA, and 2 mM salicylic acid was incubated at 30 °C for 0.5 h to allow for phosphopantetheinylation of HMWP2 and HMWP1. In the case of YbtT rescue experiments, 1.5 mM L-cysteine and 30 mM L-serine were used. Then, 50 μM YbtT, YbtT–S89A, or YbtT storage buffer (described above) was added. 10 mM ATP was immediately added to initiate the reaction, and reaction mixtures were incubated at 30 °C. 20-μl aliquots of the reactions were quenched at the designated time point with 10 μl of 10% formic acid. To extract Ybt for quantification, 100 μl of acetonitrile and 5 μl of ^{13}C-Ybt internal standard were added, and the mixtures were vortexed rigorously for 30 s; centrifuged at 14,000 × *g* for 15 min at 4 °C; and the supernatant was analyzed by LC-MS/MS (see above).

Author contributions—S. I. O. and J. P. H. conceptualization; S. I. O., Y. X., D. L. K., and M. M. investigation; S. I. O. and T. J. B. visualization; S. I. O., Y. X., and J. P. H. methodology; S. I. O., Y. X., D. L. K., T. J. B., and J. P. H. writing-original draft; S. I. O., T. J. B., and J. P. H. writing-review and editing; J. C. N. resources; J. C. N. and T. J. B. formal analysis; T. J. B. and J. P. H. supervision; T. J. B. and J. P. H. funding acquisition.

Acknowledgments—We thank Timothy Wencewicz for the ACP and Sfp expression plasmids from the Christopher Walsh lab collection. We acknowledge the Proteomics and Mass Spectrometry Facility at the Danforth Plant Science Center for identification of pulldown proteins by LC-MS/MS and their support by the National Science Foundation under Grant DBI-0922879 for acquisition of the LTQ-Velos Pro Orbitrap LC-MS/MS. Results were derived from work performed at the Advanced Light Source, Berkeley, CA (ALS). ALS is supported by the Office of Basic Energy Sciences of the United States Department of Energy Grant DE-AC02-05CH11231.

References

1. Perry, R. D., and Fetherston, J. D. (2011) Yersiniabactin iron uptake: mechanisms and role in *Yersinia pestis* pathogenesis. *Microbes Infect.* **13,** 808–817 CrossRef Medline
2. Henderson, J. P., Crowley, J. R., Pinkner, J. S., Walker, J. N., Tsukayama, P., Stamm, W. E., Hooton, T. M., and Hultgren, S. J. (2009) Quantitative metabolomics reveals an epigenetic blueprint for iron acquisition in uropathogenic *Escherichia coli*. *PLoS Pathog.* **5,** e1000305 CrossRef Medline
3. Miller, D. A., Luo, L., Hillson, N., Keating, T. A., and Walsh, C. T. (2002) Yersiniabactin synthetase: a four-protein assembly line producing the nonribosomal peptide/polyketide hybrid siderophore of *Yersinia pestis*. *Chem. Biol.* **9,** 333–344 CrossRef Medline
4. Chaturvedi, K. S., Hung, C. S., Crowley, J. R., Stapleton, A. E., and Henderson, J. P. (2012) The siderophore yersiniabactin binds copper to protect pathogens during infection. *Nat. Chem. Biol.* **8,** 731–736 CrossRef Medline
5. Koh, E. I., Robinson, A. E., Bandara, N., Rogers, B. E., and Henderson, J. P. (2017) Copper import in *Escherichia coli* by the yersiniabactin metallophore system. *Nat. Chem. Biol.* **13,** 1016–1021 CrossRef Medline
6. Robinson, A. E., Heffernan, J. R., and Henderson, J. P. (2018) The iron hand of uropathogenic *Escherichia coli*: the role of transition metal control in virulence. *Future Microbiol.* **13,** 745–756 CrossRef Medline
7. Robinson, A. E., Lowe, J. E., Koh, E. I., and Henderson, J. P. (2018) Uropathogenic enterobacteria use the yersiniabactin metallophore system to acquire nickel. *J. Biol. Chem.* **293,** 14953–14961 CrossRef Medline
8. Crosa, J. H., and Walsh, C. T. (2002) Genetics and assembly line enzymology of siderophore biosynthesis in bacteria. *Microbiol. Mol. Biol. Rev.* **66,** 223–249 CrossRef Medline
9. Meier, J. L., and Burkart, M. D. (2009) The chemical biology of modular biosynthetic enzymes. *Chem. Soc. Rev.* **38,** 2012–2045 CrossRef Medline
10. Drake, E. J., Miller, B. R., Shi, C., Tarrasch, J. T., Sundlov, J. A., Allen, C. L., Skiniotis, G., Aldrich, C. C., and Gulick, A. M. (2016) Structures of two distinct conformations of holo-non-ribosomal peptide synthetases. *Nature* **529,** 235–238 CrossRef Medline
11. Meneely, K. M., and Lamb, A. L. (2012) Two structures of a thiazolinyl imine reductase from Yersinia enterocolitica provide insight into catalysis and binding to the nonribosomal peptide synthetase module of HMWP1. *Biochemistry* **51,** 9002–9013 CrossRef Medline
12. Geoffroy, V. A., Fetherston, J. D., and Perry, R. D. (2000) *Yersinia pestis* YbtU and YbtT are involved in synthesis of the siderophore yersiniabactin but have different effects on regulation. *Infect. Immun.* **68,** 4452–4461 CrossRef Medline
13. Miller, M. C., Fetherston, J. D., Pickett, C. L., Bobrov, A. G., Weaver, R. H., DeMoll, E., and Perry, R. D. (2010) Reduced synthesis of the Ybt siderophore or production of aberrant Ybt-like molecules activates transcription of yersiniabactin genes in *Yersinia pestis*. *Microbiology* **156,** 2226–2238 CrossRef Medline
14. Lv, H., and Henderson, J. P. (2011) *Yersinia* high pathogenicity island genes modify the *Escherichia coli* primary metabolome independently of siderophore production. *J. Proteome Res.* **10,** 5547–5554 CrossRef Medline
15. Kotowska, M., and Pawlik, K. (2014) Roles of type II thioesterases and their application for secondary metabolite yield improvement. *Appl. Microbiol. Biotechnol.* **98,** 7735–7746 CrossRef Medline
16. Butler, A. R., Bate, N., and Cundliffe, E. (1999) Impact of thioesterase activity on tylosin biosynthesis in *Streptomyces fradiae*. *Chem. Biol.* **6,** 287–292 CrossRef Medline
17. Heathcote, M. L., Staunton, J., and Leadlay, P. F. (2001) Role of type II thioesterases: evidence for removal of short acyl chains produced by aberrant decarboxylation of chain extender units. *Chem. Biol.* **8,** 207–220 CrossRef Medline
18. Liu, T., You, D., Valenzano, C., Sun, Y., Li, J., Yu, Q., Zhou, X., Cane, D. E., and Deng, Z. (2006) Identification of NanE as the thioesterase for polyether chain release in nanchangmycin biosynthesis. *Chem. Biol.* **13,** 945–955 CrossRef Medline
19. Harvey, B. M., Hong, H., Jones, M. A., Hughes-Thomas, Z. A., Goss, R. M., Heathcote, M. L., Bolanos-Garcia, V. M., Kroutil, W., Staunton, J., Leadlay, P. F., and Spencer, J. B. (2006) Evidence that a novel thioesterase is responsible for polyketide chain release during biosynthesis of the polyether ionophore monensin. *Chembiochem* **7,** 1435–1442 CrossRef Medline

20. Guntaka, N. S., Healy, A. R., Crawford, J. M., Herzon, S. B., and Bruner, S. D. (2017) Structure and functional analysis of ClbQ, an unusual intermediate-releasing thioesterase from the colibactin biosynthetic pathway. *ACS Chem. Biol.* **12,** 2598–2608 CrossRef Medline
21. Mulyani, S., Egel, E., Kittel, C., Turkanovic, S., Wohlleben, W., Süssmuth, R. D., and van Pée, K. H. (2010) The thioesterase Bhp is involved in the formation of β-hydroxytyrosine during balhimycin biosynthesis in *Amycolatopsis balhimycina*. *Chembiochem* **11,** 266–271 CrossRef Medline
22. Whicher, J. R., Florova, G., Sydor, P. K., Singh, R., Alhamadsheh, M., Challis, G. L., Reynolds, K. A., and Smith, J. L. (2011) Structure and function of the RedJ protein, a thioesterase from the prodiginine biosynthetic pathway in *Streptomyces coelicolor*. *J. Biol. Chem.* **286,** 22558–22569 CrossRef Medline
23. Mady, A. S., Zolova, O. E., Millán, M. Á., Villamizar, G., de la Calle, F., Lombó, F., and Garneau-Tsodikova, S. (2011) Characterization of TioQ, a type II thioesterase from the thiocoraline biosynthetic cluster. *Mol. Biosyst.* **7,** 1999–2011 CrossRef Medline
24. Holm, L., and Laakso, L. M. (2016) Dali server update. *Nucleic Acids Res.* **44,** W351–W355 CrossRef Medline
25. Claxton, H. B., Akey, D. L., Silver, M. K., Admiraal, S. J., and Smith, J. L. (2009) Structure and functional analysis of RifR, the type II thioesterase from the rifamycin biosynthetic pathway. *J. Biol. Chem.* **284,** 5021–5029 CrossRef Medline
26. Ritchie, M. K., Johnson, L. C., Clodfelter, J. E., Pemble, C. W., 4th., Fulp, B. E., Furdui, C. M., Kridel, S. J., and Lowther, W. T. (2016) Crystal structure and substrate specificity of human thioesterase 2: insights into the molecular basis for the modulation of fatty acid synthase. *J. Biol. Chem.* **291,** 3520–3530 CrossRef Medline
27. Koglin, A., Löhr, F., Bernhard, F., Rogov, V. V., Frueh, D. P., Strieter, E. R., Mofid, M. R., Güntert, P., Wagner, G., Walsh, C. T., Marahiel, M. A., and Dötsch, V. (2008) Structural basis for the selectivity of the external thioesterase of the surfactin synthetase. *Nature* **454,** 907–911 CrossRef Medline
28. Chovancova, E., Pavelka, A., Benes, P., Strnad, O., Brezovsky, J., Kozlikova, B., Gora, A., Sustr, V., Klvana, M., Medek, P., Biedermannova, L., Sochor, J., and Damborsky, J. (2012) CAVER 3.0: a tool for the analysis of transport pathways in dynamic protein structures. *PLoS Comput. Biol.* **8,** e1002708 CrossRef Medline
29. Kozlikova, B., Sebestova, E., Sustr, V., Brezovsky, J., Strnad, O., Daniel, L., Bednar, D., Pavelka, A., Manak, M., Bezdeka, M., Benes, P., Kotry, M., Gora, A., Damborsky, J., and Sochor, J. (2014) CAVER Analyst 1.0: graphic tool for interactive visualization and analysis of tunnels and channels in protein structures. *Bioinformatics* **30,** 2684–2685 CrossRef Medline
30. Kotowska, M., Pawlik, K., Smulczyk-Krawczyszyn, A., Bartosz-Bechowski, H., and Kuczek, K. (2009) Type II thioesterase ScoT, associated with *Streptomyces coelicolor* A3(2) modular polyketide synthase Cpk, hydrolyzes acyl residues and has a preference for propionate. *Appl. Environ. Microbiol.* **75,** 887–896 CrossRef Medline
31. Tronnet, S., Garcie, C., Rehm, N., Dobrindt, U., Oswald, E., and Martin, P. (2016) Iron homeostasis regulates the genotoxicity of *Escherichia coli* that produces colibactin. *Infect. Immun.* **84,** 3358–3368 CrossRef Medline
32. Dorrestein, P. C., Bumpus, S. B., Calderone, C. T., Garneau-Tsodikova, S., Aron, Z. D., Straight, P. D., Kolter, R., Walsh, C. T., and Kelleher, N. L. (2006) Facile detection of acyl and peptidyl intermediates on thiotemplate carrier domains via phosphopantetheinyl elimination reactions during tandem mass spectrometry. *Biochemistry* **45,** 12756–12766 CrossRef Medline
33. Meluzzi, D., Zheng, W. H., Hensler, M., Nizet, V., and Dorrestein, P. C. (2008) Top-down mass spectrometry on low-resolution instruments: characterization of phosphopantetheinylated carrier domains in polyketide and non-ribosomal biosynthetic pathways. *Bioorg. Med. Chem. Lett.* **18,** 3107–3111 CrossRef Medline
34. Schwarzer, D., Mootz, H. D., Linne, U., and Marahiel, M. A. (2002) Regeneration of misprimed nonribosomal peptide synthetases by type II thioesterases. *Proc. Natl. Acad. Sci. U.S.A.* **99,** 14083–14088 CrossRef Medline
35. Reimmann, C., Patel, H. M., Walsh, C. T., and Haas, D. (2004) PchC thioesterase optimizes nonribosomal biosynthesis of the peptide siderophore pyochelin in *Pseudomonas aeruginosa*. *J. Bacteriol.* **186,** 6367–6373 CrossRef Medline
36. Bruner, S. D., Weber, T., Kohli, R. M., Schwarzer, D., Marahiel, M. A., Walsh, C. T., and Stubbs, M. T. (2002) Structural basis for the cyclization of the lipopeptide antibiotic surfactin by the thioesterase domain SrfTE. *Structure* **10,** 301–310 CrossRef Medline
37. Frueh, D. P., Arthanari, H., Koglin, A., Vosburg, D. A., Bennett, A. E., Walsh, C. T., and Wagner, G. (2008) Dynamic thiolation-thioesterase structure of a non-ribosomal peptide synthetase. *Nature* **454,** 903–906 CrossRef Medline
38. Leduc, D., Battesti, A., and Bouveret, E. (2007) The hotdog thioesterase EntH (YbdB) plays a role *in vivo* in optimal enterobactin biosynthesis by interacting with the ArCP domain of EntB. *J. Bacteriol.* **189,** 7112–7126 CrossRef Medline
39. Gulick, A. M., and Aldrich, C. C. (2018) Trapping interactions between catalytic domains and carrier proteins of modular biosynthetic enzymes with chemical probes. *Nat. Prod. Rep*. 2018, CrossRef Medline
40. Mulvey, M. A., Schilling, J. D., and Hultgren, S. J. (2001) Establishment of a persistent *Escherichia coli* reservoir during the acute phase of a bladder infection. *Infect. Immun.* **69,** 4572–4579 CrossRef Medline
41. Chen, S. L., Hung, C. S., Xu, J., Reigstad, C. S., Magrini, V., Sabo, A., Blasiar, D., Bieri, T., Meyer, R. R., Ozersky, P., Armstrong, J. R., Fulton, R. S., Latreille, J. P., Spieth, J., Hooton, T. M., *et al.* (2006) Identification of genes subject to positive selection in uropathogenic strains of *Escherichia coli*: a comparative genomics approach. *Proc. Natl. Acad. Sci. U.S.A.* **103,** 5977–5982 CrossRef Medline
42. Datsenko, K. A., and Wanner, B. L. (2000) One-step inactivation of chromosomal genes in *Escherichia coli* K-12 using PCR products. *Proc. Natl. Acad. Sci. U.S.A.* **97,** 6640–6645 CrossRef Medline
43. Gehring, A. M., Mori, I., Perry, R. D., and Walsh, C. T. (1998) The nonribosomal peptide synthetase HMWP2 forms a thiazoline ring during biogenesis of yersiniabactin, an iron-chelating virulence factor of *Yersinia pestis*. *Biochemistry* **37,** 11637–11650 CrossRef Medline
44. Suo, Z., Tseng, C. C., and Walsh, C. T. (2001) Purification, priming, and catalytic acylation of carrier protein domains in the polyketide synthase and nonribosomal peptidyl synthetase modules of the HMWP1 subunit of yersiniabactin synthetase. *Proc. Natl. Acad. Sci. U.S.A.* **98,** 99–104 CrossRef Medline
45. Quadri, L. E., Weinreb, P. H., Lei, M., Nakano, M. M., Zuber, P., and Walsh, C. T. (1998) Characterization of Sfp, a *Bacillus subtilis* phosphopantetheinyl transferase for peptidyl carrier protein domains in peptide synthetases. *Biochemistry* **37,** 1585–1595 CrossRef Medline
46. Keating, T. A., Miller, D. A., and Walsh, C. T. (2000) Expression, purification, and characterization of HMWP2, a 229-kDa, six domain protein subunit of Yersiniabactin synthetase. *Biochemistry* **39,** 4729–4739 CrossRef Medline
47. Suo, Z., Chen, H., and Walsh, C. T. (2000) Acyl-CoA hydrolysis by the high molecular weight protein 1 subunit of yersiniabactin synthetase: mutational evidence for a cascade of four acyl-enzyme intermediates during hydrolytic editing. *Proc. Natl. Acad. Sci. U.S.A.* **97,** 14188–14193 CrossRef Medline
48. Kabsch, W. (2010) XDS. *Acta Crystallogr. D Biol. Crystallogr.* **66,** 125–132 CrossRef Medline
49. McCoy, A. J., Grosse-Kunstleve, R. W., Adams, P. D., Winn, M. D., Storoni, L. C., and Read, R. J. (2007) Phaser crystallographic software. *J. Appl. Crystallogr.* **40,** 658–674 CrossRef Medline
50. Adams, P. D., Grosse-Kunstleve, R. W., Hung, L. W., Ioerger, T. R., McCoy, A. J., Moriarty, N. W., Read, R. J., Sacchettini, J. C., Sauter, N. K., and Terwilliger, T. C. (2002) PHENIX: building new software for automated crystallographic structure determination. *Acta Crystallogr. D Biol. Crystallogr.* **58,** 1948–1954 CrossRef Medline
51. Terwilliger, T. C., and Berendzen, J. (1999) Automated MAD and MIR structure solution. *Acta Crystallogr. D Biol. Crystallogr.* **55,** 849–861 CrossRef Medline
52. Emsley, P., and Cowtan, K. (2004) Coot: model-building tools for molecular graphics. *Acta Crystallogr. D Biol. Crystallogr.* **60,** 2126–2132 CrossRef Medline
53. Morin, A., Eisenbraun, B., Key, J., Sanschagrin, P. C., Timony, M. A., Ottaviano, M., and Sliz, P. (2013) Cutting edge: collaboration gets the most out of software. *eLife* **2,** e01456 CrossRef Medline
54. Meyer, P. A., Socias, S., Key, J., Ransey, E., Tjon, E. C., Buschiazzo, A., Lei, M., Botka, C., Withrow, J., Neau, D., Rajashankar, K., Anderson, K. S.,

Baxter, R. H., Blacklow, S. C., Boggon, T. J., *et al.* (2016) Data publication with the structural biology data grid supports live analysis. *Nat. Commun.* **7,** 10882 CrossRef Medline

55. Achstetter, T., Ehmann, C., and Wolf, D. H. (1981) New proteolytic enzymes in yeast. *Arch. Biochem. Biophys.* **207,** 445–454 CrossRef Medline
56. Copeland, R. A. (2002) *Enzymes*, pp. 109–145, John Wiley & Sons, Inc., New York
57. Ohlemacher, S. I., Giblin, D. E., d'Avignon, D. A., Stapleton, A. E., Trautner, B. W., and Henderson, J. P. (2017) Enterobacteria secrete an inhibitor of *Pseudomonas* virulence during clinical bacteriuria. *J. Clin. Invest.* **127,** 4018–4030 CrossRef Medline
58. Chen, D., Wu, R., Bryan, T. L., and Dunaway-Mariano, D. (2009) *In vitro* kinetic analysis of substrate specificity in enterobactin biosynthetic lower pathway enzymes provides insight into the biochemical function of the hot dog-fold thioesterase EntH. *Biochemistry* **48,** 511–513 CrossRef Medline
59. Yin, J., Lin, A. J., Golan, D. E., and Walsh, C. T. (2006) Site-specific protein labeling by Sfp phosphopantetheinyl transferase. *Nat. Protoc.* **1,** 280–285 CrossRef Medline